33RD CONGRESS
OF THE INTERNATIONAL COUNCIL
OF THE AERONAUTICAL SCIENCES
STOCKHOLM, SWEDEN, 4-9 SEPTEMBER, 2022

ICAS 2022 SWEDEN

ALTITUDE ESTIMATION BY WIDE-FIELD-INTEGRATION OF OPTIC FLOW

Hiromitsu HIRAIWA[1], Mai BANDO[1], Shinji HOKAMOTO[1]

[1]Department of Aerospace Engineering, Kyushu University,

744 Motooka, Nishi-ku, Fukuoka 819-0395 JAPAN

Abstract

In this paper, we propose an altitude estimation method by using Wide-Field-Integration (WFI) of optic flow. WFI of optic flow is a motion estimation method inspired by a biological research on the visual processing system of flying insects' compound eyes. In the standard estimation process, altitude information of a flying vehicle is necessary to estimate the motion variables of flying vehicles. The method proposed in this paper can estimate the altitude as well as the motion variables by using two patterns of optic flow acquired by two onboard cameras. The proposed method is useful for reducing onboard instrument mass and thus suitable for small autonomous vehicles. This paper discusses the mechanism of the altitude estimation and explores the suitable positions of the WFI of optic flow sensors in simulations.

Keywords: Autonomous vehicle, Optic flow, Insect vision, Altitude estimation

1. Introduction

Unmanned autonomous aircraft have made remarkable progress in recent years, and their use is being considered in a variety of fields, including goods transportation and surveillance in disaster-area. In particular, small unmanned aircraft are expected to be used for exploration of dangerous areas that are inaccessible to humans [1][2]. To realize such missions, the unmanned aircraft must be able to estimate its own attitude and motion variables with high accuracy, and they are utilized to enable stable flight. However, many autonomous navigation systems employed in unmanned aircraft rely on GPS signals, and there are challenges in GPS-denied environments such as tunnels or indoors, where GPS signals cannot reach.

As alternative sensors for autonomous flight, some missions utilize laser or image sensors. However for laser sensors, heavy weight and high energy consumption become critical problems for small UAV. For image sensors, their small-size and light-weight are preferable. However, obtaining position information from stereo-camera procedure requires large and fast computation to onboard computers.

For the reasons above, this study investigates the use of optic flow for high-speed state estimation in environments where GPS signals are not available. Optic flow is a relative velocity vector obtained from an image sensor mounted on a vehicle, but the obtained data is affected by the distance to unknown ground roughness as well as noises on images. To reduce the unknown ground and noises, Wide-Field-Integration (WFI) of optic flow has been proposed to estimate the velocity and angular velocity of the aircraft by integrating a wide range of these vectors [3][4]. The WFI of optic flow has the following favorable characteristics for autonomous unmanned aircraft, such that it uses only image sensors with small-size and light-weight, and that the computational load required in estimation process is small and fast.

We have been continuing research to implement the WFI of optic flow theory by using practical engineering devices for small unmanned aircraft. However, the altitude information of aircraft is

necessary to estimate its motion variables in the theory, and this indicates that the aircraft must equip with an altimeter. Therefore, this paper proposes a method to estimate altitude by using two patterns of optic flow. This method enables the construction of a simpler and lighter sensor system without an altimeter. This paper verifies the validity of the proposed method and investigates the effect of camera placement by computer simulations.

2. Motion estimation method using optic flow

2.1 Optic flow

Optic flow is a velocity vector field obtained by an image sensor, as shown in Figure 1. According to camera motion, corresponding pixel positions are identified by performing image processing such as a gradient method and a block-matching method on these multiple images. Note that the image processing methods used in this process are less computational demanding than the stereo method dealing with millions of pixel data.

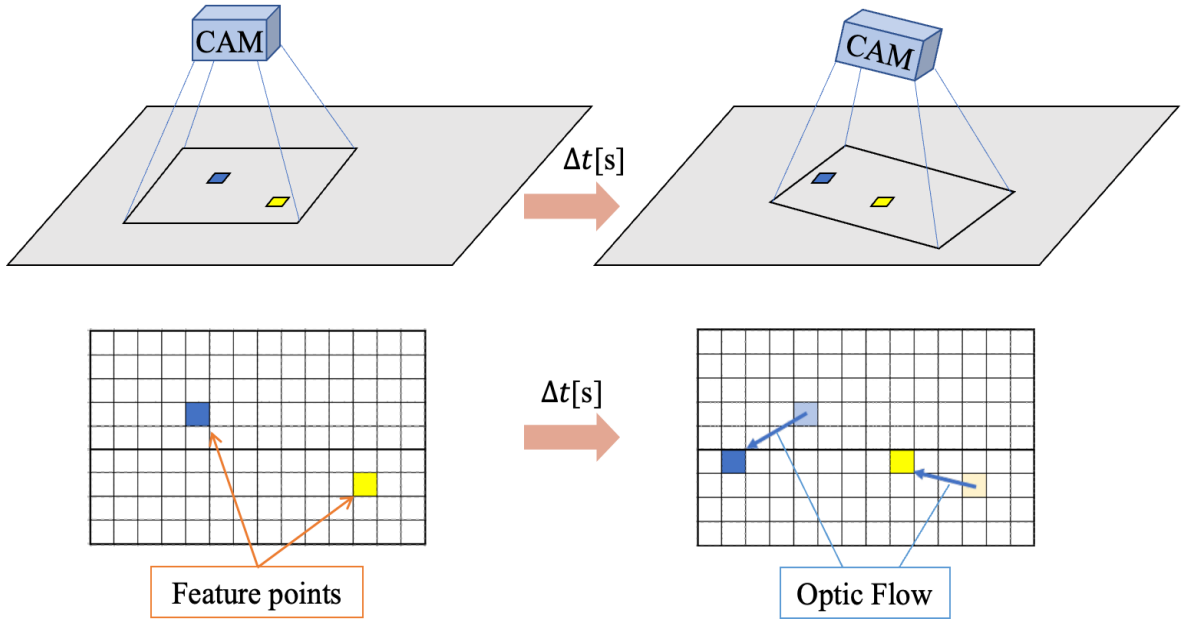

Figure 1 – Schematic diagram for optic flow

2.2 Modeling of optic flow

As shown in Figure 2, an aircraft with an image sensor placed at its center of gravity is considered for optic flow modelling. In this case, the vector $\boldsymbol{Q}$ from the origin to a point on the unit sphere constructed around the image sensor is shown as follows.

$$\boldsymbol{Q} = [\sin\beta\cos\gamma \quad \sin\beta\sin\gamma \quad \cos\beta]^T \tag{1}$$

where γ is the azimuth angle from the x_b axis and β is the depression angle from the z_b axis. Optic flow is the velocity vector obtained on the sphere, and is outputs with two components, as $\dot{\boldsymbol{Q}} = [\dot{Q}_\gamma \quad \dot{Q}_\beta]^T$. The relative velocity field, $\dot{\boldsymbol{Q}}$, can be expressed as

$$\dot{\boldsymbol{Q}} = -\boldsymbol{\omega} \times \boldsymbol{Q} - \mu[\boldsymbol{v} - (\boldsymbol{v}^T\boldsymbol{Q})\boldsymbol{Q}] \tag{2}$$

where $\boldsymbol{v} = [u \quad v \quad w]^T$[m/s] is the translational velocity, $\boldsymbol{\omega} = [p \quad q \quad r]^T$[rad/s] is the angular velocity defined in the body coordinate system. The μ is called the nearness function and the inverse of the distance d_{pho} [m] from the image sensor to a feature point in the environment. For a virtually assumed infinite horizontal plane, the nearness function μ is

$$\mu = \frac{\lambda(\phi,\theta)}{d_{pho}} = \frac{-s\beta c\gamma s\theta + s\beta s\gamma s\phi c\theta + c\beta c\phi c\theta}{d_{pho}} \tag{3}$$

Here, ϕ and θ are the roll and pitch angles of the aircraft in 3-2-1 Euler angle representation, d is the altitude of the aircraft, and $\mathrm{c}(*) = \cos(*), \mathrm{s}(*) = \sin(*)$.

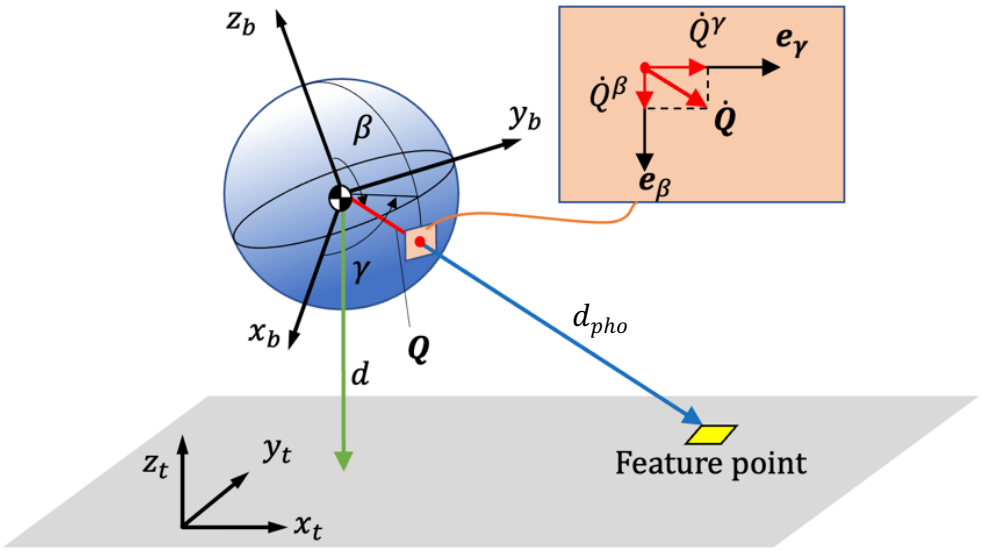

Figure 2 – Geometric relation for coordinate systems and image surface

2.3 WFI of optic flow

WFI of optic flow is a method for accurately estimating the motion variables of an aircraft by integrating a wide range of optic flows. To combine the optic flow over the spherical surface, the WFI of optic flow requires a sensitivity function to integrate the acquired optic flows. Since the spherical image is two-dimensional surface, spherical harmonic functions are used for the sensitivity function $\boldsymbol{F}$ to perform the integration process [5][6]. The output $\boldsymbol{y}$ can be expressed as in the following equation.

$$\boldsymbol{y} = \begin{bmatrix} \boldsymbol{y}^\gamma \\ \boldsymbol{y}^\beta \end{bmatrix} = \int_S \dot{\boldsymbol{Q}} \boldsymbol{F}\, d\boldsymbol{\Omega} = \int_S \dot{\boldsymbol{Q}} \begin{bmatrix} \boldsymbol{F}^\gamma & \boldsymbol{0} \\ \boldsymbol{0} & \boldsymbol{F}^\beta \end{bmatrix} d\boldsymbol{\Omega} \tag{4}$$

where S represents the entire spherical image plane and $d\Omega$ is the solid angle of the sphere. Spherical harmonic can be defined as the functions of higher order. Therefore, using sensitivity functions up to the Mth order, $\boldsymbol{y}^\beta$ and $\boldsymbol{y}^\gamma$ are vectors with dimensions of the Mth order, as in Equations (5) and (6).

$$\boldsymbol{y}^\gamma = \left[\int_S \dot{\boldsymbol{Q}}_\gamma \boldsymbol{F}_1^\gamma\, d\boldsymbol{\Omega} \quad \cdots \quad \int_S \dot{\boldsymbol{Q}}_\gamma \boldsymbol{F}_M^\gamma\, d\boldsymbol{\Omega} \right]^T \tag{5}$$

$$\boldsymbol{y}^\beta = \left[\int_S \dot{\boldsymbol{Q}}_\beta \boldsymbol{F}_1^\beta\, d\boldsymbol{\Omega} \quad \cdots \quad \int_S \dot{\boldsymbol{Q}}_\beta \boldsymbol{F}_M^\beta\, d\boldsymbol{\Omega} \right]^T \tag{6}$$

Therefore, the output $\boldsymbol{y}$ is a $2M \times 1$ vector. In the standard procedure for WFI of optic flow, it is assumed that optic flow is measured at continuous points. However, in actual systems, optic flow is obtained as discrete data. Shoemaker and Hokamoto [7] proposed to replace the integral operation in calculating the output $\boldsymbol{y}$ with a Riemann sum, and showed that such a replacement does not degrade the accuracy of the estimation. Therefore, the actual output of WFI of optic flow can be calculated as

$$\boldsymbol{y}^{\gamma} = \begin{bmatrix} \sum_{k=1}^{N} \dot{\boldsymbol{Q}}_{\gamma}(\boldsymbol{\gamma}_k, \boldsymbol{\beta}_k) \boldsymbol{F}_1^{\gamma}(\boldsymbol{\gamma}_k, \boldsymbol{\beta}_k) \Delta\boldsymbol{\Omega}_k \\ \vdots \\ \sum_{k=1}^{N} \dot{\boldsymbol{Q}}_{\gamma}(\boldsymbol{\gamma}_k, \boldsymbol{\beta}_k) \boldsymbol{F}_M^{\gamma}(\boldsymbol{\gamma}_k, \boldsymbol{\beta}_k) \Delta\boldsymbol{\Omega}_k \end{bmatrix} \tag{7}$$

$$\boldsymbol{y}^{\beta} = \begin{bmatrix} \sum_{k=1}^{N} \dot{\boldsymbol{Q}}_{\beta}(\boldsymbol{\gamma}_k, \boldsymbol{\beta}_k) \boldsymbol{F}_1^{\beta}(\boldsymbol{\gamma}_k, \boldsymbol{\beta}_k) \Delta\boldsymbol{\Omega}_k \\ \vdots \\ \sum_{k=1}^{N} \dot{\boldsymbol{Q}}_{\beta}(\boldsymbol{\gamma}_k, \boldsymbol{\beta}_k) \boldsymbol{F}_M^{\beta}(\boldsymbol{\gamma}_k, \boldsymbol{\beta}_k) \Delta\boldsymbol{\Omega}_k \end{bmatrix} \tag{8}$$

where N is the total number of optic flows obtained from the image sensors.The obtained output $\boldsymbol{y}$ is linear for the velocity and angular velocity of the aircraft. Assuming that the motion variable of the aircraft is $\boldsymbol{x} = [u \quad v \quad w \quad p \quad q \quad r]^T$, the output $\boldsymbol{y}$ of the WFI of Optic flow can be expressed as the following relation.

$$\boldsymbol{y} = \boldsymbol{C}(\phi, \theta, d)\boldsymbol{x} \tag{9}$$

where the matrix $\boldsymbol{C}$ is a $2M \times 6$ matrix. When ϕ, θ, and d are obtained from a gyro sensor or an altimeter, the motion variable vector $\boldsymbol{x}$ can be estimated by using the pseudo-inverse $\boldsymbol{C}^{\dagger}$ for the full rank matrix $\boldsymbol{C}$ as follows.

$$\boldsymbol{x} = \boldsymbol{C}(\phi, \theta, d)^{\dagger}\boldsymbol{y} \tag{10}$$

3. Altitude estimation method using WFI of optic flow

3.1 Optic flow outside the body center of gravity

As shown in Figure 3, a second camera sensor (Camera 2) is introduced to estimate the altitude d by utilizing WFI of optic flow process. Since this camera sensor is at a point apart from the body

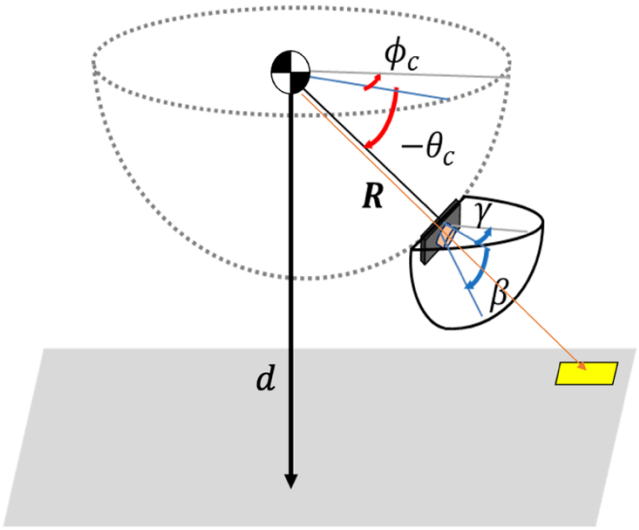

Figure 3 – Coordinate system of CAM2

center of gravity of the aircraft, the equation of optic flow is different from Equation (2). Given that the camera is mounted at a point with a distance R [m] from the body center of gravity and whose azimuth and depression angles are ϕ_c [rad] and θ_c [rad] respectively, the optic flow can be expressed by the following coefficient matrices $\boldsymbol{A}$, $\boldsymbol{B}$, and $\boldsymbol{C}$ as

$$\dot{\boldsymbol{Q}} = \boldsymbol{A\omega} + \frac{\lambda}{z - R\cos\theta_c}(\boldsymbol{Bv} + R\boldsymbol{BC\omega})$$
$$\boldsymbol{A} = \begin{bmatrix} c\beta c\gamma & c\beta s\gamma & -s\beta \\ s\gamma & -c\gamma & 0 \end{bmatrix}, \boldsymbol{B} = \begin{bmatrix} s\gamma & -c\gamma & 0 \\ c\beta c\gamma & c\beta s\gamma & -s\beta \end{bmatrix}, \boldsymbol{C} = \begin{bmatrix} 0 & c\theta_C & -s\theta_C s\phi_C \\ -c\theta_C & 0 & s\theta_C c\phi_C \\ s\theta_C s\phi_C & -s\theta_C c\phi_C & 0 \end{bmatrix} \quad (11)$$

3.2 Altitude estimation

The motion estimation method described in Chapter 2 assumes that the camera is installed at the aircraft's center of gravity. Assuming that the d is an unknown variable, the motion variable cannot be estimated because the matrix $\boldsymbol{C}$ in Equation (10) cannot be calculated. However, the matrix $\boldsymbol{C}$ can be calculated by including the d into $\boldsymbol{x}$. Therefore, even if the altitude is unknown, the ratio $\boldsymbol{V}(= [U \quad V \quad W]^T = [u/d \quad v/d \quad w/d]^T$)of the relative translational velocity to the altitude, and the angular velocity $\boldsymbol{\omega}(= [p \quad q \quad r]^T$) can be estimated using the WFI of optic flow. The optic flow obtained by Camera 2 can be arranged by the variable as shown in the following equation.

$$\dot{\boldsymbol{Q}}d + (R\cos\theta_c\,\boldsymbol{A} - R\boldsymbol{\lambda BC})\boldsymbol{\omega} - \lambda\boldsymbol{Bv} - \boldsymbol{A\omega}d = R\cos\theta_c\dot{\boldsymbol{Q}} \quad (12)$$

Unknown variables in this equation are d, $\boldsymbol{v}$, and $\boldsymbol{\omega}$. When the angular velocity $\boldsymbol{\omega}$ is estimated from Camera 1, since the translational velocity can be expressed as $\boldsymbol{v} = \boldsymbol{V}d$, the remained unknown variable is only the distance d in the following equation:

$$\dot{\boldsymbol{Q}}d + (R\cos\theta_c\,\boldsymbol{A} - R\lambda\boldsymbol{BC})\boldsymbol{\omega} - \lambda\boldsymbol{BV}d - \boldsymbol{A\omega}d = R\cos\theta_c\dot{\boldsymbol{Q}} \quad (13)$$

Calculating the Riemann sum in the image area of Camera 2 and integrating the optic flow yields Equation (14).

$$\boldsymbol{\Sigma\dot{Q}\Delta\Omega_2}d + \boldsymbol{\Sigma}(R\cos\theta_c\,\boldsymbol{A} - R\lambda\boldsymbol{BC})\boldsymbol{\Delta\Omega_2\omega} - \boldsymbol{\Sigma}\lambda\boldsymbol{B\Delta\Omega_2 V}d - \boldsymbol{\Sigma A\Delta\Omega_2\omega}d = \boldsymbol{\Sigma}R\cos\theta_c\dot{\boldsymbol{Q}}\,\boldsymbol{\Delta\Omega_2} \quad (14)$$

By arranging Equation (14) with respect to the d, the azimuth and depression direction components yield the equation for distance estimation as

$$\boldsymbol{d} = \begin{bmatrix} d_\gamma \\ d_\beta \end{bmatrix} = \frac{\boldsymbol{\Sigma}R\cos\theta_c\dot{\boldsymbol{Q}}\,\boldsymbol{\Delta\Omega_2} - \boldsymbol{\Sigma}(R\cos\theta_c\,\boldsymbol{A} - R\lambda\boldsymbol{BC})\boldsymbol{\Delta\Omega_2\omega}}{\boldsymbol{\Sigma\dot{Q}\Delta\Omega_2} - \boldsymbol{\Sigma}\lambda\boldsymbol{B\Delta\Omega_2 V} - \boldsymbol{\Sigma A\Delta\Omega_2\omega}} \quad (151)$$

Finally, the translational velocity $\boldsymbol{v}$ can also be calculated by computing the product of $\boldsymbol{V}$ and d estimated by Camera 1. Thus, by using two cameras, the proposed method can estimate the altitude in addition to the angular velocity and translational velocity of the aircraft.

3.3 Numerical Simulation

In order to verify the validity of the proposed method, numerical simulations are applied for a flying UAV. The simulation conditions are shown in Table 1 and Figure 4. Fig. 4(a) shows the layout of the two cameras: top-view (left) and side-view (right), and Fig. 4(b) illustrates an image of the UAV motion. A typical simulation result is shown in Fig. 5. In this simulation, noises with a mean value of 0 and standard deviation of 0.03 [rad/s] are added to ideal optic flow; note these noises are specified from our experimental devices. As shown in Fig. 5(g), the altitude estimated and the other motion variables show reasonable results. Note that the d is calculated as the average of d_β and d_γ . This means that the proposed method is valid.

Table 1 Flight condition of a vehicle (Case 1)

Altitude	d	[m]	2
Attitude angle	$(\phi \quad \theta \quad \psi)$	[deg.]	$(0 \quad 0 \quad 0)$
Translation motion	$(u \quad v \quad w)$	[m/s]	$(1 \quad 1 \quad 0)$
Angular velocity	$(p \quad q \quad r)$	[rad/s]	$(0 \quad 0 \quad 0)$

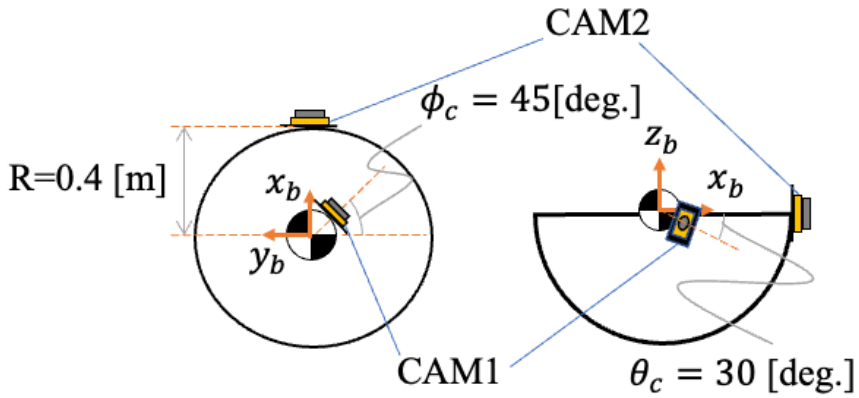

(a) – Camera layout (left: top-view, right: side-view)

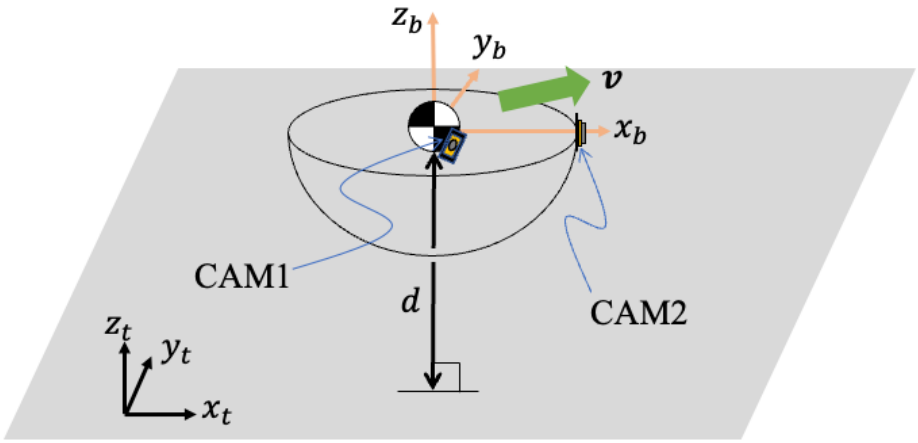

(b) – Bird's-eye view for a moving vehicle

Figure 4 – Illustration showing the geometric relation between the vehicle and two cameras.

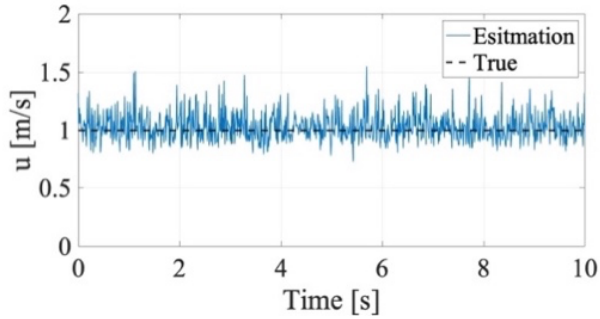

(a) – translational velocity u

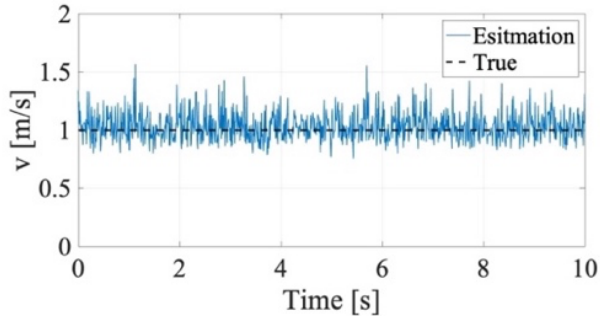

(b) – translational velocity v

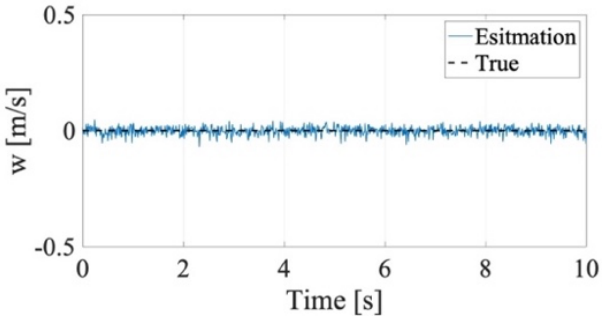

(c) – translational velocity w

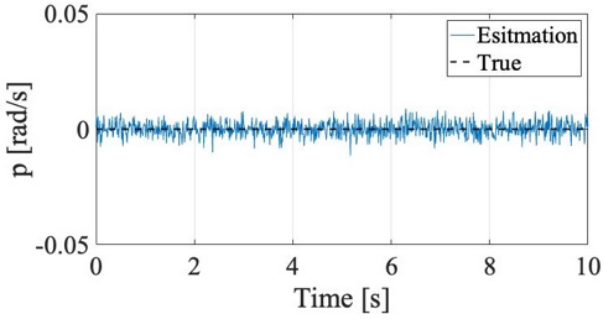

(d) – angular velocity p

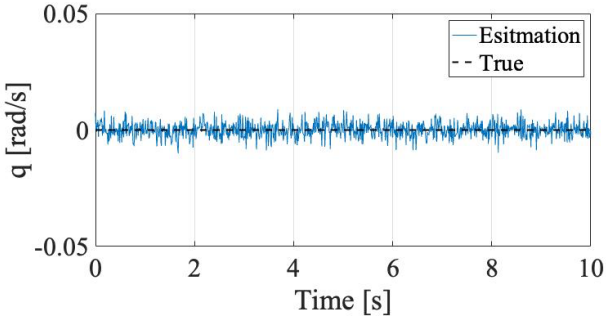

(e) – angular velocity q

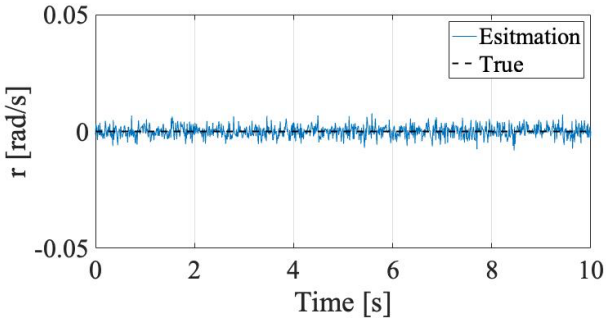

(f) – angular velocity r

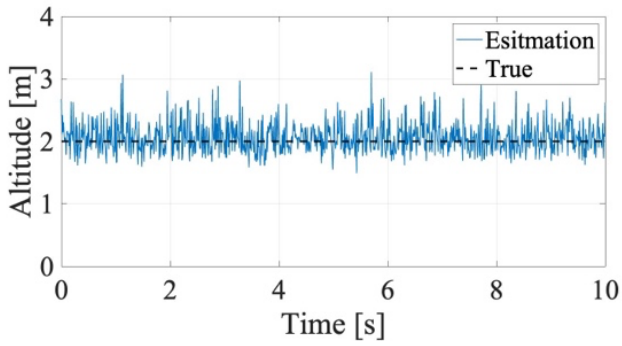

(g) – altitude d (average of d_β and d_γ)

Figure 5 – Time histories for the estimated moving variables and altitude.

4. Effect of camera placement on estimation accuracy

4.1 Assumptions

For better implementation of the proposed method in a system, it is necessary to clarify the relationship between camera placement and estimation accuracy. In the numerical simulation shown in Chapter 3, the aircraft is in translational motion without changing its attitude or altitude, and the distance between each camera and the ground is equal. Therefore, the same optic flow pattern is obtained by each camera. In this case, as shown in Fig. 5, the altitude estimation is still possible although two optic flow patterns are similar. This implies that the proposed method does not estimate the altitude by using the differences in the obtained optic flow patterns. Instead, we presume that the distance R between Camera 1 and Camera2 may affect the accuracy of the estimation and evaluate the accuracy in the following simulation.

4.2 Numerical Simulation

Table 2 Flight condition of a vehicle (Case 2)

Altitude	d	[m]	2
Attitude angle	$(\phi \quad \theta \quad \psi)$	[deg.]	$(0 \quad 0 \quad 0)$
Translation motion	$(u \quad v \quad w)$	[m/s]	$(2 \quad 2 \quad 0)$
Angular velocity	$(p \quad q \quad r)$	[rad/s]	$(0 \quad 0 \quad 0)$

f

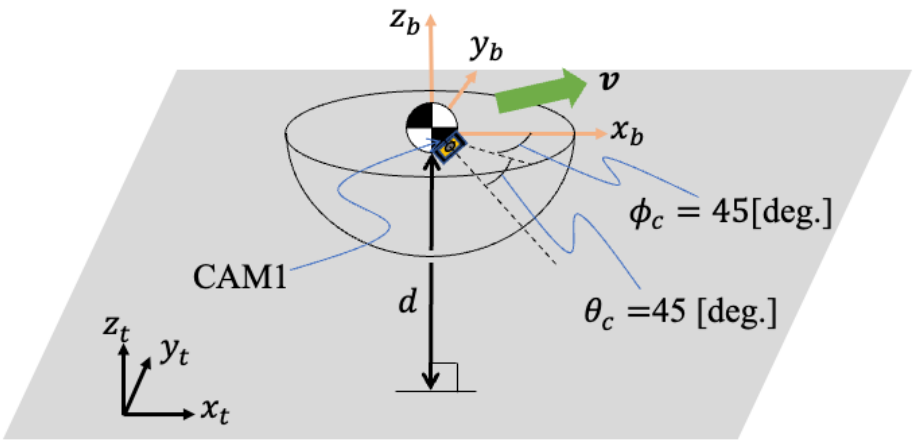

(a) – Bird's-eye view for a moving vehicle

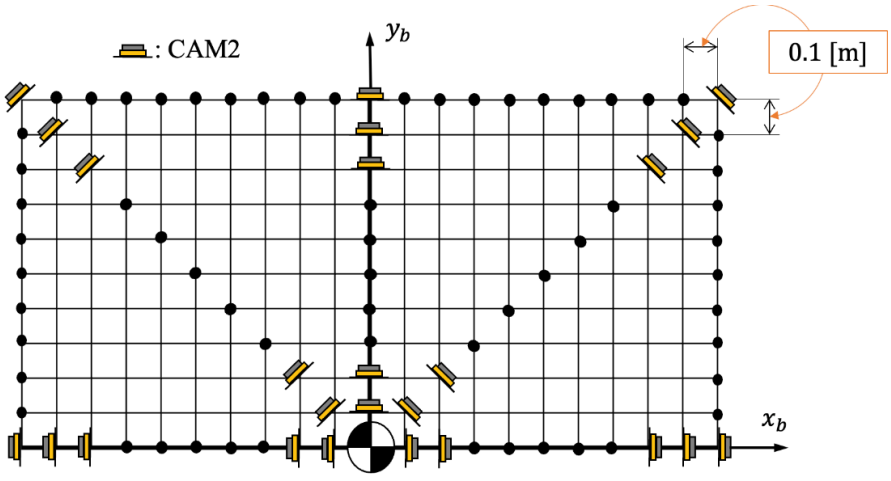

(b) – The second camera layout

Figure 6 – Geometry of the vehicle motion and camera layout.

Numerical simulations are performed for the motion shown in Table2. As shown in Figure 6(a), Camera 1 is fixed at the center of gravity position for simplicity with $\phi = 45\ [\mathrm{deg.}],\ \theta = 45\ [\mathrm{deg.}]$. As shown in Figure 6(b), the position of Camera 2 is changed -1 [m] ~ 1 [m] in $x_b$axis and 0 [m] ~ 1 [m] in y_b axis with 0.1 [m] interval. To reduce the effect of random noises, the estimation is performed 10 times at each position. In this simulation, the same noise as in Chapter 3 is added to the ideal optic flow. The estimation accuracy is evaluated by calculating the variance of the error between the estimated result and the true value as follows:

$$d_{std} = \frac{1}{n}\sum(d_{estimate} - d_{true})^2 \tag{16}$$

Numerical simulation results are shown in Fig. 7. Yellow areas indicate d_{std} values greater than 0.5 (poor accuracy), and the closer to blue, the lower the d_{std} value becomes (good accuracy). This result indicates that the accuracy improves as the position of Camera 2 moves away from Camera 1 located at the origin. The only difference in the optic flow obtained from each camera used for estimation is the R, and therefore, the estimation accuracy of the proposed method can be improved by increasing the distance between the two cameras.

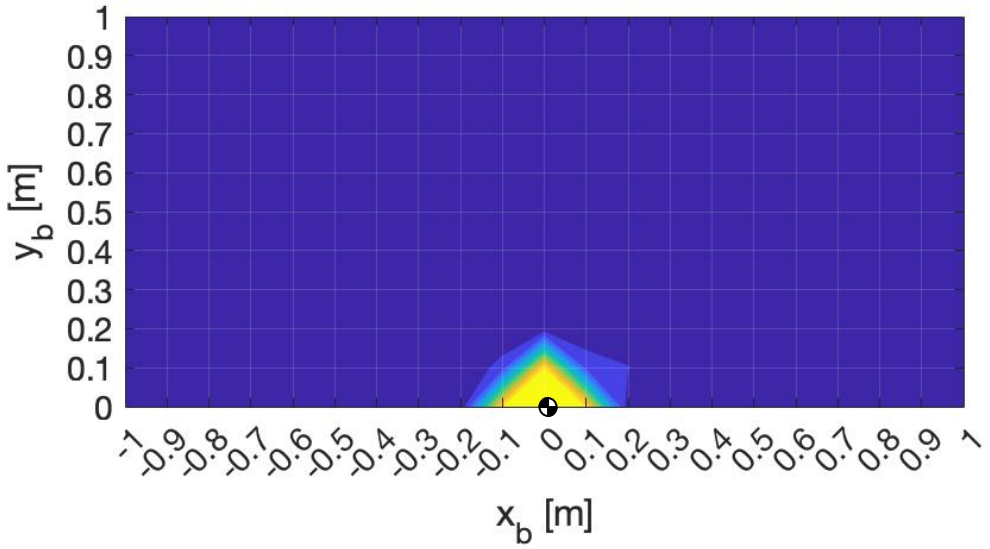

(a) – Evaluation of estimated d_γ

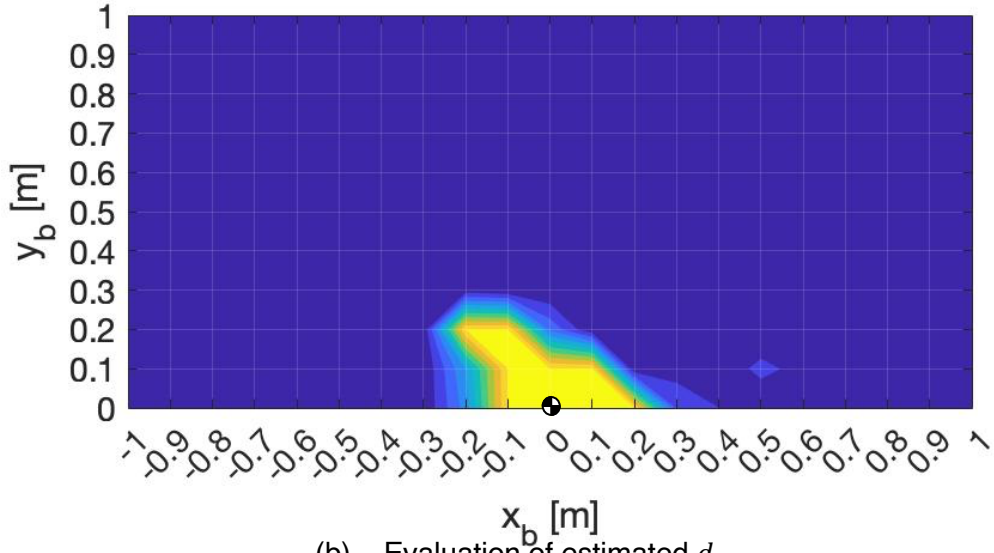

(b) – Evaluation of estimated d_β

Figure 7 – Evaluation results for the estimation accuracy.

5. Conclusion

In this paper, we proposed an altitude estimation using WFI of optic flow and verified its validity and estimation accuracy. First, an altitude estimation method using two patterns of optic flow was proposed, and it was confirmed that the estimation is possible even when noise is added. This method has the potential to construct a simpler and lighter sensor system without using an altimeter. Then, it was shown that the proposed method is affected by the distance between the two cameras in the estimation accuracy through the numerical simulations. It indicates that increasing the distance between multiple cameras in the system configuration can improves the estimation accuracy. This result will be helpful when constructing the actual system.

6. Acknowledgement

This work was supported by JSPS KAKENHI Grant Number JP20H02354.

7. Contact Author Email Address

The contact author: Hiromitsu HIRAIWA

email address: hiraiwa.hiromitsu.824@s.kyushu-u.ac.jp

8. Copyright Statement

References

[1] Shaojie Shen., Nathan Michael. and Vijay Kumar, Autonomous Multi-Floor Indoor Navigation with a Computationally Constrained MAV', *IEEE International Conference on Robotics and Automation*, pp. 20-25 (2011).

[2] D. David, S. Jorg, and S. Behnke, Local Multi-Resolution Surfel, Grids for MAVMotion Estimation and 3D Mapping, *Proceedings of 13th International Conference on Intelligent Autonomous Systems*, pp. 429–442 (2014).

[3] Humbert, J. S. and Hyslop, A. M., Bio-Inspired Visuomotor Convergence, IEEE Transactions on Robotics, Vol. 26, pp. 121-130 (2010).

[4] Hyslop, A. M. and Humbert, J. S., Autonomous Navigation in Three-Dimensional Urban Environments Using Wide-Field Integration of Optic Flow, Journal of Guidance, Control, and Dynamics, Vol. 33, pp. 147-159 (2010).

[5] Kobayashi, N., Bando, M. and Hokamoto, S., Improvement of Wide-Field-Integration of Optic Flow Considering Practical Sensor Restrictions, Journal of Mechanical Engineering and Automation, Vol. 7, No. 2, pp. 53-62 (2017).

[6] Naoto Kobayashi, Mai Bando, Shinji Hokamoto, Daisuke Kubo, Guidelines for Practical Navigation Systems Based on Wide-Field-Integration of Optic Flow, Asian Journal of Control, pp. 2381-2392 (2021)

[7] Shoemaker, M. A. and Hokamoto, S., Comparison of Integrated and Nonintegrated Wide-Field Optic Flow for Vehicle Navigation, Journal of Guidance, Control, and Dynamics, Vol. 36, pp. 710-720 (2013).